JACS
JOURNAL OF THE AMERICAN CHEMICAL SOCIETY

Article

pubs.acs.org/JACS

Synergy between Experimental and Computational Chemistry Reveals the Mechanism of Decomposition of Nickel–Ketene Complexes

Nicholas D. Staudaher, Atta M. Arif, and Janis Louie*

Department of Chemistry, The University of Utah, 315 S 1400 E, Salt Lake City, Utah 84112, United States

Supporting Information

ABSTRACT: A series of (dppf)Ni(ketene) complexes were synthesized and fully characterized. In the solid state, the complexes possess η^2-(C,O) coordination of the ketene in an overall planar configuration. They display similar structure in solution, except in some cases, the η^2-(C,C) coordination mode is also detected. A combination of kinetic analysis and DFT calculations reveals the complexes undergo thermal decomposition by isomerization from η^2-(C,O) to η^2-(C,C) followed by scission of the C═C bond, which is usually rate limiting and results in an intermediate carbonyl carbene complex. Subsequent rearrangement of the carbene ligand is rate limiting for electron poor and sterically large ketenes, and results in a carbonyl alkene complex. The alkene readily dissociates, affording alkenes and (dppf)Ni(CO)$_2$. Computational modeling of the decarbonylation pathway with partial phosphine dissociation reveals the barrier is reduced significantly, explaining the instability of ketene complexes with monodentate phosphines.

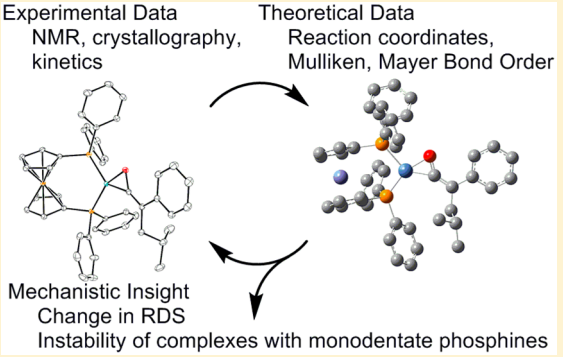

INTRODUCTION

Ni–Ketene complexes are highly probable reaction intermediates in the carbonylation[1] of diazo compounds,[2] Danheiser benzannulations,[3] [2 + 2 + 2] cycloadditions of diynes and ketenes,[4] and, importantly, the Fisher–Tropsch reaction.[5] As such, some effort has gone into developing methods for synthesizing Ni–ketene complexes and, furthermore, understanding their fundamental reactivity. Unfortunately, effective and general syntheses to these complexes are still lacking. For example, only a handful of Ni–ketene complexes (e.g., complexes **1**–**7**) have been successfully prepared to date (Figure 1) and complex **7**[6] has not been fully characterized. Furthermore, many of these complexes are unstable at ambient conditions thereby hampering detailed reactivity studies.

To further complicate matters, Ni–ketene complexes tend to decompose to form catalytically incompetent Ni–CO complexes. Miyashita and co-workers showed that the decomposition of complex **1a**, which is stable at −30 °C, at room temperature[7] affords $(PPh_3)_2Ni(CO)_2$ as well as styrene and but-2-ene-2,3-diyldibenzene as organic byproducts (Figure 1). They propose the decomposition proceeds by an isomerization from η^2-(C,O) to η^2-(C,C) followed by scission of the C═C bond, forming a carbonyl carbene complex. In contrast to the instability of complexes **1**–**3**, compounds **4**–**6**[8] are stable at room temperature. Although the thermal decomposition of complexes **5**[9] and **6**[10] were not evaluated, complex **4** decomposes over 24 h at 80 °C.

Despite the lack of information on Ni–ketene complexes, Ir– and Rh–ketene complexes have been studied in much more depth and lend insight into the decomposition of Ni–ketene complexes. In fact, coordination through both the C═

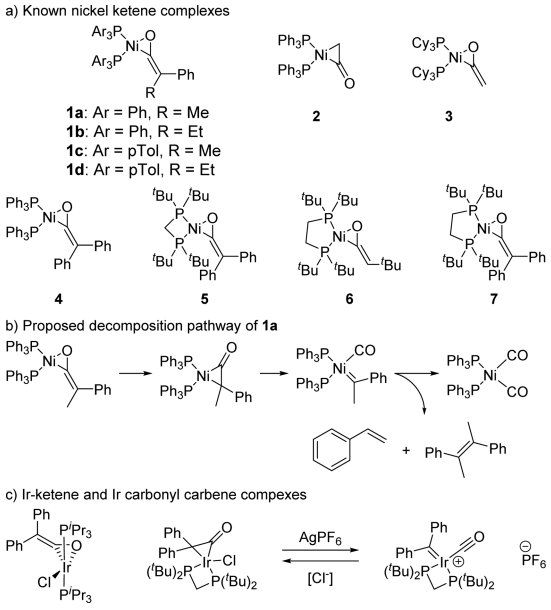

Figure 1. Known Ni–ketene complexes and proposed decomposition pathway.

Received: August 24, 2016
Published: September 30, 2016

DOI: 10.1021/jacs.6b08897
J. Am. Chem. Soc. 2016, 138, 14083–14091

O[11] and C=C[12] bonds of a ketene have been observed in Ir complexes. Furthermore, the scission of the C=C bond to form an Ir carbonyl carbene complex has been shown to be reversible and has been studied in depth computationally.[13] (Figure 1c).

The decomposition of Ni–ketene complexes to Ni–CO complexes is particularly intriguing considering the lack of Ni–CO intermediates in many reaction mechanisms that likely involve Ni–ketene complexes. That is, formation of Ni–CO would prevent product formation in these reactions. Thus, it may be possible that Ni–CO complexes form reversibly in some cases or, more likely, Ni–ketene complexes with higher stability have rates of reactions that are faster than rates of decomposition to Ni–CO. Clearly, a deeper understanding regarding the conversion of Ni–ketene complexes to Ni–CO complexes could aid in the development of new Ni–mediated chemistries of ketenes. Herein we report a detailed evaluation of the structure and mechanism of decomposition of (dppf)-Ni(ketene) complexes.

RESULTS

Synthesis of (dppf)Ni(ketene) Complexes. Our initial efforts focused on the synthesis of a library of Ni–ketene complexes that are stable at room temperature but decompose upon heating. Since all known Ni–ketene complexes have phosphines as supporting ligands, we began by screening the reaction of a variety of monodentate and bidentate phosphine ligands with $Ni(COD)_2$ and butyl phenyl ketene (eq 1). Not

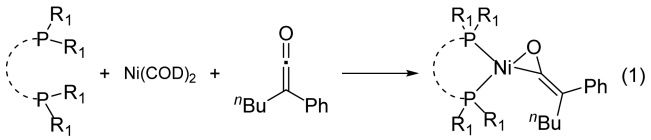

(1)

surprisingly, the use of a monodentate phosphine such as PPh_3 did not afford a long-lived Ni–ketene complex at room temperature as determined by $^{31}P\{^1H\}$ NMR and IR spectroscopy. Indeed, carbonyl peaks, 2002 and 1944 cm^{-1}, were observed and are consistent with the formation of decomposition product $(PPh_3)_2Ni(CO)_2$.[14]

Various bidentate phosphine ligands were also examined. To our dismay, reactions run with dppe, dppp, dppb, or dppbenzene with $Ni(COD)_2$ and diphenylketene also did not afford the desired Ni–ketene complexes. Instead, a mixture of $LNi(COD)$ and L_2Ni species were observed by $^{31}P\{^1H\}$ NMR spectroscopy as we have seen with Xantphos.[15] The formation of these species were confirmed by omitting ketene from the reactions, which led to identical $^{31}P\{^1H\}$ NMR spectra. Furthermore, in the reaction with dppe, only a broad singlet at 44.6 ppm, which is consistent with $(dppe)_2Ni$, was observed.[16] The formation of bis-chelated species is detrimental to Ni–ketene complex formation because for every L_2Ni species, an equivalent of $Ni(COD)_2$ is left over which reacts rapidly with ketene to form nickel carbonyl compounds.[8]

Gratifyingly, the reaction between dppf and $Ni(COD)_2$ formed (dppf)Ni(COD) quantitatively, observed as a sole singlet at 34 ppm in the $^{31}P\{^1H\}$ NMR spectrum; $(dppf)_2Ni$ was not observed.[17] Furthermore, when phenyl butyl ketene was added to a solution of $Ni(COD)_2$ and dppf that was allowed to equilibrate for 60 s, clean formation of Ni–ketene **8b** occurred as indicated by the disappearance of the singlet at 34 ppm and the appearance of two doublets at 42 and 17 ppm, consistent with inequivalent phosphines of a Ni–ketene complex (*vide infra*). Butyl phenyl ketene could be substituted with other alkyl aryl ketenes (eq 2) under similar reaction conditions to afford a series of (dppf)Ni(ketene) complexes that were easily recrystallized from pentane (Table 1).

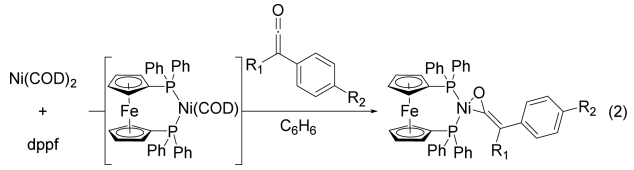

Table 1. Yields of Ketene Complexes

complex	R_1	R_2	yield (%)
8a	Ph	H	85
8b	*n*Bu	H	79
8ca	*i*Bu	F	76
8cb	*i*Bu	H	67
8cc	*i*Bu	Me	75
8cd	*i*Bu	OMe	37
8d	*i*Pr	H	80
8e	*s*Bu	H	78

Crystallography. Solid state structures for a variety of complexes are shown in Figure 2, and selected bond distances and lengths are in Table 2. The structure of **8a** is planar about the Ni center, and the ketene is bound through the C=O bond. The phenyl ring containing C(9) is nearly in plane with the ketene fragment, with a O(1)–C(1)–C(2)–C(9) dihedral angle of −4.6(4)°, indicating the p orbitals of the ketene and the arene are in conjugation. The other ketene phenyl ring, which contains C(3), is in a π-stacking[18] interaction with the ring containing C(15) on the dppf fragment. The centroid-centroid distance is 3.644 Å and the planes are skewed by 7.38°.

The structure of **8b** is, unfortunately, disordered. The unit cell contains four complexes, with random orientation of each ketene fragment relative to the unit cell, i.e., a given unit cell may have all butyl chains down, and another all up, or any combination thereof. As such, **8b** appears to have C_2 symmetry about the line containing the Fe and Ni atoms. Thermal ellipsoids of some carbon atoms have therefore been omitted from Figure 2b for clarity, and reliable bond lengths and angles for the metallaoxirane cannot be obtained. Nevertheless, the X-ray structure clearly demonstrates that the ketene is C=O bound; the phenyl ring is oriented away from the dppf fragment and almost in plane with the C=C bond.

The structures of **8e**, **8ca**, **8cb**, and **8cc** show similar features in that they are planar, bound through the C=O fragment of the ketene, and have the aromatic ring in plane with the ketene. Interestingly, the structures of **8ca**, **8cb**, and **8cc** reveal that the O(1)–C(1)–C(2)–C(7) dihedral angle increases with more electron rich aromatic rings, indicating slightly better orbital overlap with electron poor ketenes. Also, the O(1)–Ni–C(1) angle decreases slightly from **8ca** to **8cc**, indicating tighter binding of the C=O fragment with electron poor ketenes. The fact that aryl alkyl ketenes have the arene oriented away from the Ni center indicates that the orbital overlap between the arene and the ketene is energetically more favorable than the π-stacking interaction in the structure of **8a**. Finally, the P(1)-Ni (trans to O) bond length is slightly shorter than the P(2)-Ni

DOI: 10.1021/jacs.6b08897
J. Am. Chem. Soc. 2016, 138, 14083–14091

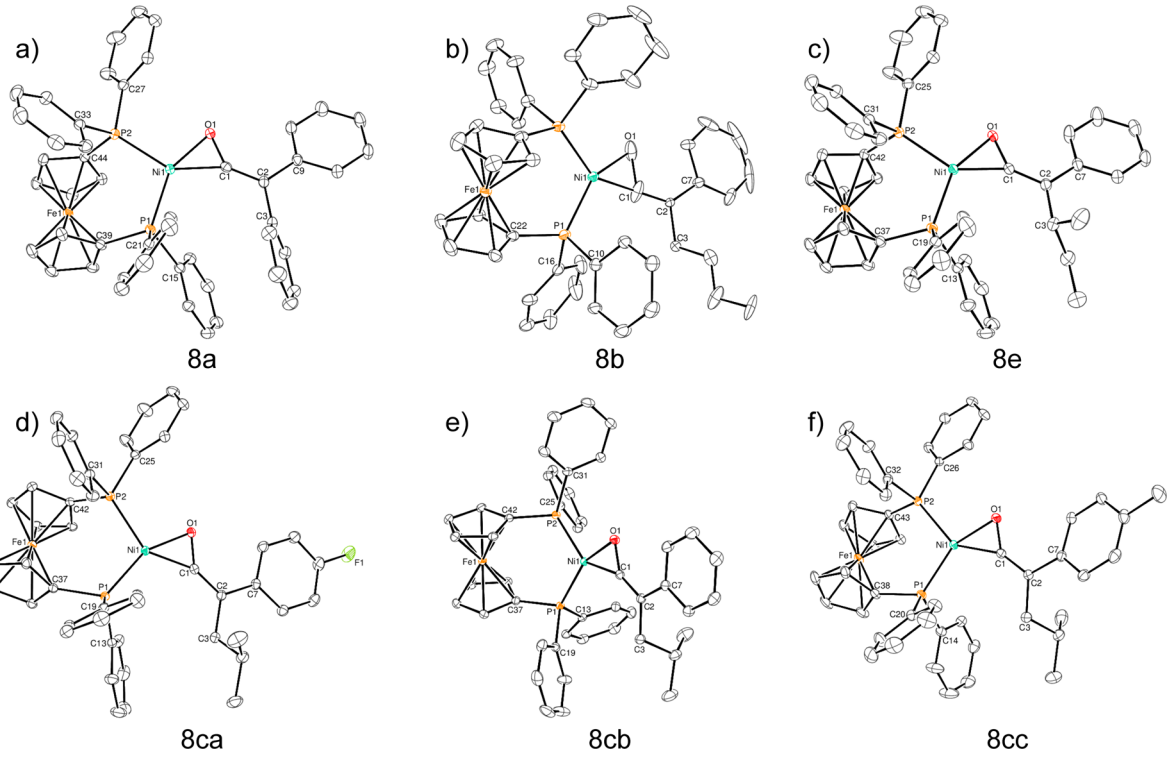

Figure 2. ORTEP diagrams of (dppf)Ni(ketene) complexes. Ellipsoids are set at 30% probability.

Table 2. Selected Bond Lengths, Angles, and Torsions of (dppf)Ni(ketene) Complexes

complex	P_1–Ni	P_2–Ni	Ni–O_1	Ni–C_1	O_1–C_1	C_1–C_2	O_1–Ni–C_1	P_1–Ni–P_2	O_1–C_1–C_2–C_7
8a	2.1557(6)	2.2252(6)	1.866(1)	1.875(2)	1.297(3)	1.350(3)	40.59(7)	105.60(2)	−4.6(4)
8b	2.1832(15)	2.1833(15)	1.862(5)	1.862(5)	1.383(14)	1.291(11)	43.6(4)	108.13(8)	−19(1)
8e	2.1488(7)	2.2151(7)	1.861(2)	1.878(2)	1.292(2)	1.352(3)	40.42(7)	105.18(2)	−7.1(4)
8ca	2.1551(5)	2.2293(5)	1.851(1)	1.887(2)	1.293(2)	1.352(2)	40.46(6)	104.86(2)	−2.0(3)
8cb	2.1569(6)	2.2306(6)	1.855(1)	1.886(2)	1.292(2)	1.354(3)	40.41(7)	104.78(2)	3.0(3)
8cc	2.1568(5)	2.2277(6)	1.871(1)	1.878(2)	1.291(2)	1.350(3)	40.28(7)	106.34(2)	6.2(3)

(trans to C(1)) bond, revealing a modest trans effect. The Ni–O bonds are shorter than the Ni–C bonds, indicating tighter binding of the O atom than the C.

Spectroscopy. The $^{31}P\{^1H\}$ NMR spectrum of **8b** contains two doublets at 42 and 17 ppm with a coupling constant of 23 Hz, consistent with a planar Ni complex with *cis* phosphines and an unsymmetrical π substituent that does not rotate freely. The aromatic region of the ^1H NMR spectrum is complicated, but the cyclopentadienyl region clearly shows four signals between 4.3–3.6 ppm, consistent with a dppf ligand containing mirror symmetry about the plane containing the Fe and P atoms. In addition, the alkyl region contains signals corresponding to an *n*-butyl chain. The $^{13}C\{^1H\}$ spectrum contains a doublet at 168.7 (J = 48 Hz) corresponding to the ketene O=***C***=C carbon and a doublet of doublets at 79.3 ppm (J = 7, 4 Hz) consistent with the O=C=***C*** carbon. The IR spectrum of **8b** contains only one carbonyl peak at 1624 cm^{-1}, consistent with a C=O coordinated ketene.

Interestingly, the spectral data for **8ca** are much more complicated. The $^{31}P\{^1H\}$ NMR spectrum (Figure 3) displays two doublets at 40.8 and 17.3 ppm (J = 22 Hz) as well as two much smaller doublets, each slightly upfield of the first set of doublets, at 40.2 and 17.0 ppm (J = 21 Hz) and a singlet at 23.5 ppm (Figure 3), indicative of three coordination modes of the ketene. The ^1H NMR spectrum is also consistent with three

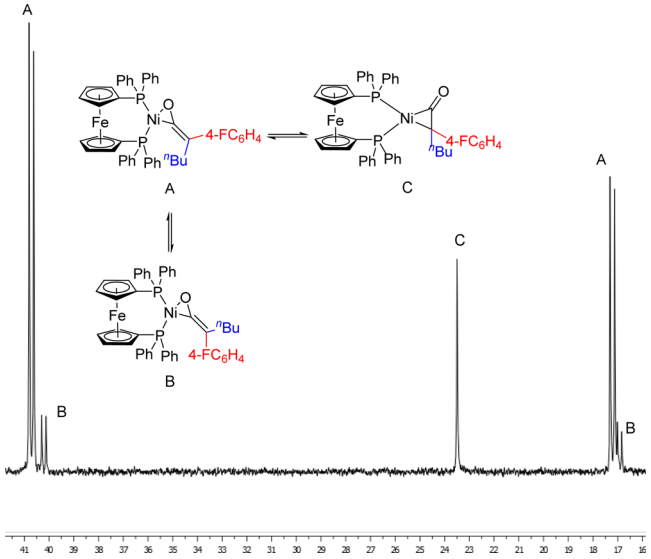

Figure 3. $^{31}P\{^1H\}$ spectrum and coordination modes of **8ca**.

structural isomers. The Cp region displays this behavior more clearly than the aromatic or alkyl regions. There are three sets of four signals, with integrations 25:4:2; one each of the largest

DOI: 10.1021/jacs.6b08897
J. Am. Chem. Soc. 2016, 138, 14083–14091

and second largest peaks overlap. The IR spectrum shows two carbonyl peaks at 1597 and 1743 cm^{-1}. The largest signals in the $^{31}P\{^1H\}$ NMR and ^1H NMR spectra and the carbonyl stretch at 1597 cm^{-1} correspond to a (dppf)Ni–ketene complex where the ketene is C=O coordinated and the aromatic ring is oriented away from the dppf fragment (A, Figure 3). This orientation matches what is seen in the solid state by X-ray crystallography. Based on the similarity in chemical shifts and coupling constants, the doublets at 40.2 and 17.0 ppm in the $^{31}P\{^1H\}$ NMR spectrum and the smallest set of peaks in the ^1H NMR spectrum likely correspond to the coordination mode where the ketene is still C=O coordinated but the aromatic ring is oriented toward the dppf fragment and the isobutyl chain is distal to the Ni center (B, Figure 3). Finally, we attribute the singlet that appears at 23.5 ppm in the $^{31}P\{^1H\}$ NMR, the second set of peaks in the Cp region of the ^1H NMR, and the carbonyl stretch at 1743 cm^{-1} to the coordination mode where the ketene is C=C coordinated (C, Figure 3), which is often the case in Ir and Rh ketene complexes.[11,12,19] The $^{13}C\{^1H\}$ NMR spectrum of complex **8ca** lacks the signal-to-noise to see all the peaks for the three coordination modes. Only one carbonyl peak is observed, a ddd at 169.1 ppm (J_{PC} = 41, 7 Hz; J_{FC} = 1 Hz), which we attribute to the coordination mode observed in the solid state (A). The O=C=***C*** carbon gives rise to a doublet of doublets at 76.7 ppm (J_{PC} = 8, 6 Hz). However, the carbon *meta* to fluorine displays a set of three doublets between 117 and 114 ppm, one of each corresponding to each coordination mode. To our knowledge, this is the first example of multiple coordination modes of ketenes observed simultaneously, although it is similar to the coordination of *α,β*-unsaturated aldehydes and ketones to $CpRe(NO)(PPh_3)^+$.[20]

Kinetics of Decomposition. The rates of decomposition of **8b–e** were measured by ^1H NMR at 100 °C in toluene-d_8 (eq 3). The reaction is first order overall and therefore first

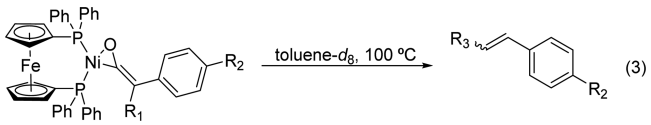

(3)

order in ketene complex with half-lives between 0.48–2.5 h, indicating these complexes are quite stable to thermal decomposition compared to **1a**. A 1:1 mixture of *cis*- and *trans*-alkene products was observed in the decomposition of **8b**. Furthermore, the kinetic isotope effect was investigated by monitoring the decomposition of **8b** and its analogue with a fully deuterated *n*-butyl chain, **8b-*d*$_9$** (Table 3, entries 1 and 2). A k_H/k_D = 1.35 is observed, consistent with secondary kinetic isotope effects, and indicates that in the rate-determining step the C–H bond is not broken and that the O=C=***C*** carbon undergoes a change in hybridization. Increasing steric bulk of the alkyl chain from *n*-butyl to *i*-butyl (entry 4) decreases the stability of the complex, but increasing the steric size of the chain to isopropyl (entry 7) gave a rate constant in-between the *n*-butyl and *i*-butyl. Electronic effects were also investigated with isobutyl alkyl chains. Increasing the donating character from R_2 = H to Me and to OMe (entries 4–6) increases the stability of the complex, and these three data points produce a near perfect Hammett plot with ρ = 2.31 vs σ_p (Figure 4).

Table 3. Kinetics of Decomposition of (dppf)Ni(ketene) Complexes

entry	complex	R_1	R_2	K_{obs} ($\times 10^{-4}$/s)
1	**8b**	^{n}Bu	H	1.0377(5)
2	**8b-*d*$_9$**	^{n}Bu-d_9	H	0.771(15)
3	**8ca**	^{i}Bu	F	0.997(81)
4	**8cb**	^{i}Bu	H	5.02(26)
5	**8cc**	^{i}Bu	Me	3.57(32)
6	**8cd**	^{i}Bu	OMe	2.69(26)
7	**8d**	^{i}Pr	H	2.40(9)

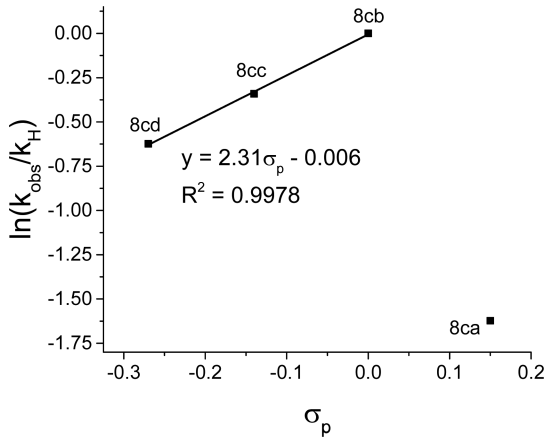

Figure 4. Linear free relationship for decomposition of electron neutral and rich (dppf)Ni(aryl isobutyl ketene) complexes.

These data suggests that negative charge is built up on the O=C=***C*** carbon of the ketene in the rate-determining step of the reaction. However, complex **8ca** (entry 3) is an outlier of this relationship, indicating the mechanism of decomposition for this complex is different or has a different rate-determining step. Unfortunately, complex **8e** was not kinetically competent. Significant line broadening was observed within the first few time points, indicative of paramagnetic product formation.

Calculation of the Reaction Coordinate. The mechanism of decomposition of complex **8b** was studied by DFT calculations to gain further insight into the structures and energies of the intermediates and transition states (Figure 5). We found the BP86 functional and a split basis set consisting of tzvp for Ni, P, and the O=C=C fragment and svp for all other atoms reproduced the crystal structure of **8cb**, and this level of theory was used for optimizations and frequency calculations in the study of the decomposition of **8b**. BLYP/6-31G* gave an energy of C=C coordinated complex **9** that was slightly higher than **8b**, consistent with our observation of this species spectroscopically for **8ca**, and the energy of **TS2** (which our experimental data indicates is rate limiting, *vide infra*) that aligned well with the experimental activation energy. Several higher levels of theory were evaluated for single point energy calculations, and they failed to accurately predict these energies (see SI for further computational details and benchmarking). Complex **8b** isomerizes from C=O coordination to C=C coordination (**9**) through **TS1**. The C=C bond is then cleaved, leading to carbonyl carbene complex **10** through **TS2**. The energy of this transition state, 28.7 kcal/mol agrees with the experimental activation energy of 28.8 kcal/mol, and this step has the largest individual barrier (26.8 kcal/mol) along the calculated pathway. A previous report has found that (dtbpe)Ni(η^2-(*C*,*C*)-O=C=CH_2) undergoes C–C scission

DOI: 10.1021/jacs.6b08897
J. Am. Chem. Soc. 2016, 138, 14083–14091

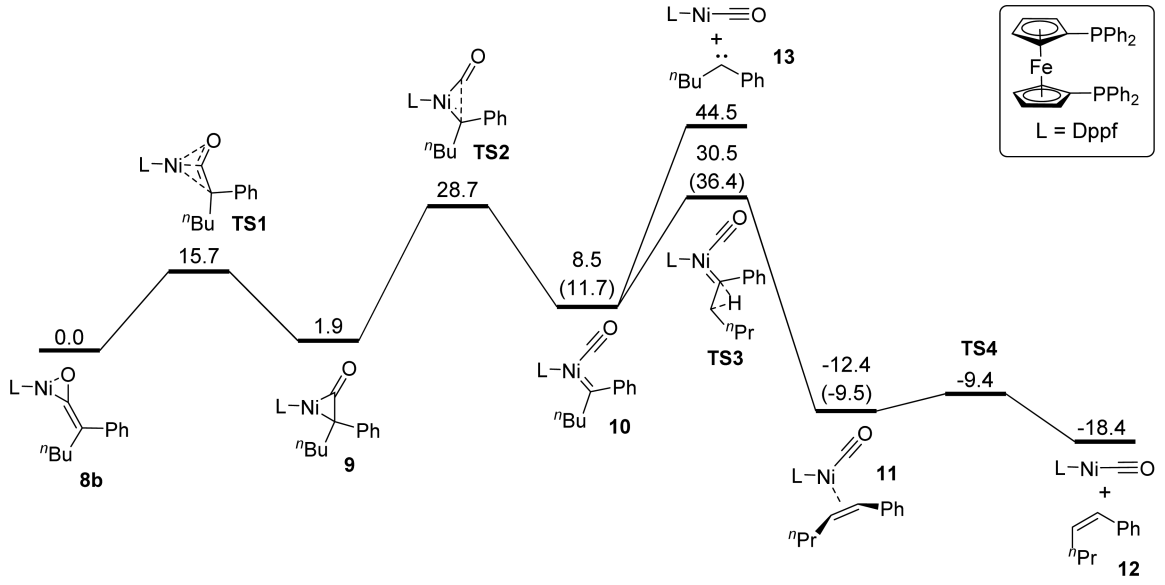

Figure 5. Calculated reaction coordinate for the decomposition of **8b**. Optimizations were carried out with BP86/tzvp-svp and single point energies were located with BLYP/6-31G*. Units are in kcal/mol relative to **8b**. Numbers in parentheses are for formation of the *trans* alkene, where formation of the *cis* alkene is shown.

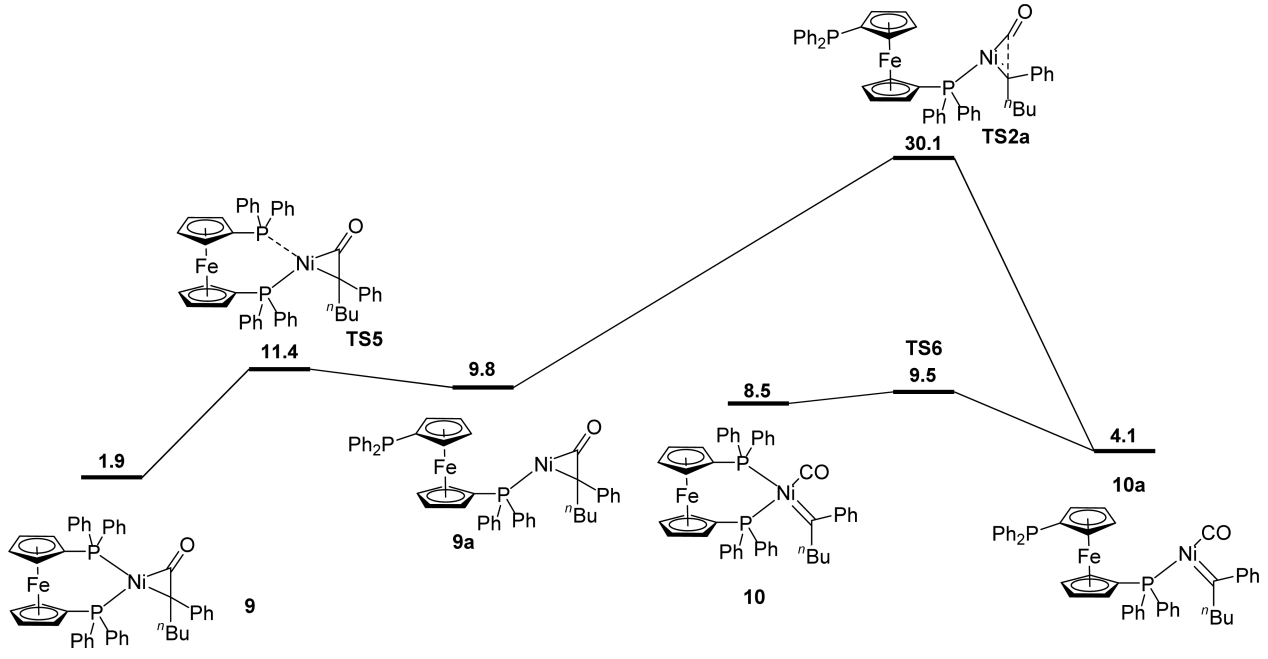

Figure 6. Role of partial phosphine dissociation for C═C coordinated ketene complexes, carbonyl carbene complex, and decarbonylation. Energies are in kcal/mol relative to the energy of **8b**.

with a $\Delta G^{\ddagger}$ of 41.6 kcal/mol and a ΔG of 38.8 kcal/mol.[21] These numbers are at odds with our theoretical and experimental work, albeit (dtbpe)Ni(O═C═CH_2) is significantly different than our complexes and that work was benchmarked to the dissociation of CO from $Ni(CO)_4$. Subsequent to the decarbonylation event, the carbene rearranges to an alkene via hydrogen transfer in **TS3**. The barrier for this step is 22.0 kcal/mol for the *cis* alkene and 24.7 kcal/mol for the *trans* alkene. Furthermore, the conformation of **10** leading to the *trans* alkene is 3.2 kcal/mol higher in energy than that leading to the *cis* alkene. These barriers for hydrogen migration are less than the barrier for decarbonylation by 2.1−4.8 kcal/mol for the *trans* and *cis* alkenes, respectively. Nevertheless, these transition states represent the second highest individual barrier and the highest point on the reaction coordinate.

We also investigated carbene dissociation of **10** to **13**, which is strongly uphill in energy and therefore not relevant to the decomposition pathway. Complex **11** then undergoes an exergonic alkene dissociation to form three-coordinate (dppf)-Ni(CO), which is highly reactive and explains the observation of (dppf)$Ni(CO)_2$ by IR in samples subjected to kinetic analysis.

In addition, we investigated the possible role of partial phosphine dissociation in each step. Dissociation of one P atom from the C═O coordinated complex **8b** was found to be

DOI: 10.1021/jacs.6b08897
J. Am. Chem. Soc. 2016, 138, 14083−14091

endergonic by 22.2 kcal/mol. Given the lower energy required to reach **TS1**, we believe dissociation of a phosphine from **8b** is irrelevant to the mechanism. In contrast, phosphine dissociation from C═C coordinated complex **9** may be thermodynamically and kinetically competent (Figure 6). The barrier for decarbonylation with one P atom coordinated (**9a**) is 20.3 kcal/mol, significantly less than the experimental activation energy of 28.4 kcal/mol. However, the barrier for reassociation of the tethered phosphine arm in complex **9a** is only 1.9 kcal/mol. Furthermore, phosphine dissociation from the carbonyl carbene complex **10** has a barrier of only 1.0 kcal/mol (to **TS6**) and is actually downhill in energy by 4.4 kcal/mol (to **10a**). The transition states for hydride transfer with partial phosphine dissociation are 35.0 and 34.6 kcal/mol relative to **8b** for the *cis* and *trans* alkenes, respectively, and the conformation of the carbonyl carbene complex that leads to the *cis* alkene is 1.5 kcal/mol higher in energy than that leading to the *trans* alkene (Figure 7).

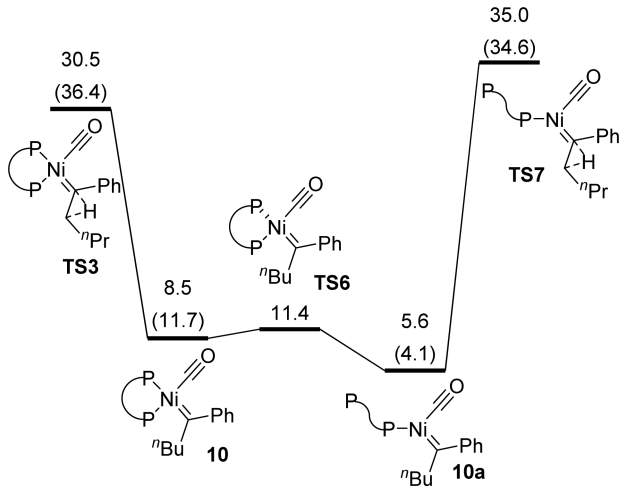

Figure 7. Reaction paths for hydride migration, leading to *cis* and *trans* alkenes. Numbers in parentheses are for the *trans* alkene. Energies are in kcal/mol relative to **8b**.

DISCUSSION

Resting State of Multiple Coordination Modes of the Ketene. The spectral and crystallographic data of our ketene complexes indicate that the C═O coordination mode with the ketene's aryl group oriented away from the Ni atom is the thermodynamic minimum. In the solid state, the aromatic group of the ketene is oriented away from the Ni atom and the alkyl group is toward the (dppf)Ni fragment. The spectral data of **8ca** indicate the existence of two other coordination modes that have similar energies to the isomer observed in the solid state. The first of these is also CO coordinated, with the aryl and alkyl groups interchanged such that the alkyl group is oriented away from the Ni atom and the arene is in the π-stacking interaction with one of the dppf phenyl rings (B, Figure 3). Our calculations indicate this coordination mode is 2.6 kcal/mol higher in energy for complex **8b**. The third isomer has the ketene coordinated via the C═C bond (C, Figure 3). Isomer C gives a singlet in the $^{31}P\{^{1}H\}$ NMR, indicating that the ketene is freely rotating. The calculated energy of **9** relative to **8b** (1.9 kcal/mol) also corroborates the assignment of our spectral data to this coordination mode. Furthermore, the calculated barrier for isomerization of **8b** to **9** of 15.7 kcal/mol agrees well with the experimental barrier of 14 kcal/mol for the isomerization of **1a** based on line broadening in the ^{1}H spectrum at low temperature.[7]

Evidence for Rate Limiting Decarbonylation. Our calculations indicate that the decarbonylation step has the highest barrier for an individual step in the pathway, and that the hydride migration is the highest point on the pathway thereby restricting the possible rate-determining step to these two options. The kinetic isotope effect observed for **8b** and **8b-d_9** (1.35) rules out C−H bond scission in the rate-determining step, and is consistent with several β and γ secondary KIEs associated with rehybridization of the O═C═***C*** carbon during the rate-determining step. Mayer bond order analysis suggests a change of hybridization occurs for the O═C═***C*** carbon during decarbonylation: the difference in C═C bond order in complex **9**, which is 0.948, and the free ketene, which is 1.564, indicates significant back bonding into the C═C bond and that the hybridization of the O═C═***C*** carbon of complex **9** lies in-between sp^3 and sp^2, while in complex **10**, this carbon is a carbene, which is sp^2 hybridized. Furthermore, the value of ρ (2.31) indicates significant buildup of negative charge on the O═C═***C*** carbon during the rate-determining step for complexes **8cb**−**8cd**. Mulliken analysis of intermediates associated with decarbonylation and hydride transfer shows significant buildup of negative charge on the O═C═***C*** carbon atom during decarbonylation and not during hydride migration. This carbon atom has a −0.19 charge in C═C coordinated complex **9**, −0.36 in carbonyl carbene complex **10**, and −0.38 in carbonyl alkene complex **11**. The buildup of charge on this carbon during decarbonylation can be easily rationalized since it gains a lone pair. Thus, the combination of KIE and linear free energy relationship (LFER) analysis, aided by DFT calculations, indicate decarbonylation is rate-limiting in most cases. We benchmarked our single point energies accordingly, and the fit is excellent. Applying the rates derived from the DFT calculations to the steady state approximation (eq 4) for an equilibrium between C═O and C═C coordinated ketene complexes followed by scission of the C═C bond (eq 5) gives a rate constant of 1.28×10^{-4} Hz, which is in excellent agreement with experimental rate of 1.038×10^{-4} Hz. This indicates that our computational model fits the kinetic data very well and that decarbonylation is rate limiting for complex **8b**. Furthermore, Mulliken analysis reveals that **8b** and **9** are essentially Ni(II) species, whereas **10** is nearly Ni(0). Decarbonylation is therefore a reductive process with regard to the Ni center, and we predict that more electron donating phosphines will stabilize Ni−ketene complexes even more effectively than dppf.

$$k = \frac{k_1 k_2 [\mathbf{8b}]}{k_{-1} + k_2} \tag{4}$$

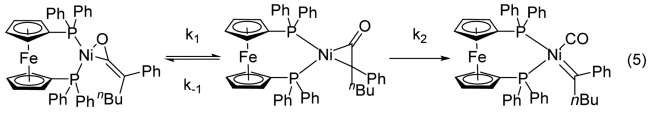

(5)

Mechanism of Hydrogen Atom Migration. Following decarbonylation, the carbene ligand rearranges to an alkene. To do so, the β hydrogen must migrate to the α carbon. A close examination of transition state **TS3-*cis*** (Figure 8) shows the migrating hydrogen atom is orthogonal to the nodal plane of the π-bond that is formed. Thus, the hydrogen transfer involves orbital overlap between the carbene sp^2 orbital that contains the

DOI: 10.1021/jacs.6b08897
J. Am. Chem. Soc. 2016, 138, 14083−14091

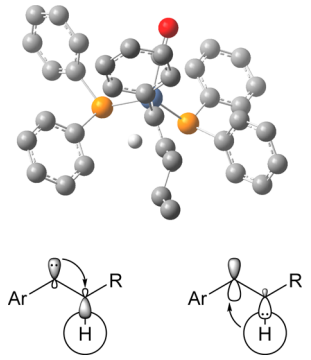

Figure 8. **TS3-*cis*** and simplified orbital interactions of carbonyl carbene complex leading to hydride transfer. Ferrocene and most H atoms omitted for clarity.

lone pair and the C−H σ^* as well as overlap between the filled C−H σ and empty carbene p orbitals. Consequently, the transfer involves a hydride rather than a proton or an H•. However, from our computational model it is difficult to say if this step occurs with or without phosphine dissociation. Application of the Curtin-Hammett principle to the energies associated with hydride transfer with both phosphine associated (*vide supra*) gives a *cis*:*trans* ratio of 49:1. A ratio of 1:2 is predicted with partial phosphine dissociation, albeit the barriers for hydride migration with one phosphorus coordinated to Ni are unrealistically high. It is difficult to be certain where the error in our computational model is either the barriers for hydride transfer with partial phosphine dissociation or the $\Delta\Delta G^{\ddagger}$ for the *cis* and *trans* alkene isomers without partial phosphine dissociation have been overestimated.

Hydride Transfer Is Rate-Limiting in Some Cases. Complex **8ca**, which possesses an electron withdrawing *p*-fluorophenyl on the ketene, is a clear outlier of the LFER (Figure 4). Extrapolation of the LFER gives a rate of decarbonylation of 7.06×10^{-4} Hz, significantly faster than the observed rate. The reason decomposition is much slower for this complex is likely two-fold. First, the electron withdrawing group allows for greater stabilization of the buildup of negative charge on the O=C=***C*** carbon during decarbonylation thereby enhancing the rate of this step. Furthermore, the hydride migration step is attenuated by electron withdrawing groups. That is, the nucleophilicity of the carbene sp^2 orbital containing the lone pair and the electrophilicity of the empty carbene p orbital are both attenuated by the electron withdrawing group. We therefore believe **8ca** defies the LFER because of accelerated decarbonylation and decelerated hydride migration to the point where hydride migration, rather than decarbonylation, is rate-limiting.

Another outlier of the trends associated with ketene complex decomposition is complex **8d**. Though the electronic character between complexes **8b**, **8cb**, and **8d** are the same, the steric bulk of the alkyl substituent steadily increases (i.e., *n*-butyl < *i*-butyl < *i*-propyl) yet the rate of decomposition both increases then decreases for this series of complexes. That is, complex **8cb** decomposes ∼5 fold faster than complex **8b**; yet complex **8d**, which one would expect to have an even higher rate of decomposition than complex **8cb**, decomposes ∼2 fold slower than complex **8cb** (i.e., rates of decomposition display the following trend: **8b** < **8cb** > **8d**). Along these lines, complex **8e** would be predicted to have a slower rate of decomposition than **8cb** and **8d**. However, kinetic analysis of complex **8e** was unsuccessful; significant amounts of paramagnetic Ni species were produced. It is possible that the increased steric bulk of the ethyl of the *s*-butyl group, relative to the methyl of the *i*-propyl group, is sufficiently large enough to destabilize complex **9** such that homolytic cleavage of the Ni−C bond and radical reactions occurs.

Our calculations suggest that a deviation in the rate-limiting step for the decomposition of complex **8d**, as well as **8ca**, occurs, albeit for two different reasons. In these cases, hydrogen migration is rate determining. Inspection of complex **10** (the carbonyl carbene complex of **8b**) (Figure 9) reveals that this

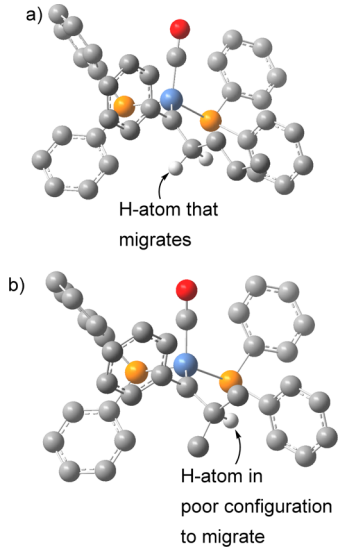

Figure 9. (a) **10**, the carbonyl carbene complex of **8b**, (b) carbonyl carbene complex of **8d**.

intermediate has the orbital overlap necessary for hydride migration (*vide supra*) in its lowest energy conformation. The Ni−C−C−H dihedral of complex **10** is −122.84°, similar to that of **TS3-*cis***, which has a dihedral of −81.33°, a difference of less than an anti−gauche isomerization. On the other hand, the carbonyl carbene complex of **8d** has a Ni−C−C−H dihedral of −9.90°, indicating that this complex must undergo significant rotation about the C−C bond to adopt the orbital overlap necessary for hydride transfer. Furthermore, rotation of the isopropyl group is significantly more energetically demanding than for an *n*- or isobutyl group. We therefore propose that the hydrogen migration is rate limiting with large alkyl groups (such as those in **8d**) as well as electron withdrawing groups (such as those in **8ca**).

Decarbonylation with Partial Phosphine Dissociation Is Relevant for Monodentate Phosphines. Despite the lower barrier for the decarbonylation step with one phosphine associated, partial phosphine dissociation is clearly not relevant to the decomposition of ketene complexes with bidentate phosphines. Applying the steady state approximation rate equation (eq 4) to the reaction in eq 6, where an equilibrium exists between the C=C coordinated complex with either one or two phosphines associated, followed by decarbonylation gives a k_{obs} of 1.83×10^{-5} Hz, which is ∼5 fold slower than the experimental rate. Nevertheless, this pathway could be highly relevant for ketene complexes with monodentate phosphines, which are known to be quite unstable. When the phosphine is not tethered to the complex (eq 7) phosphine dissociation is entropically favored thereby increasing the population of

DOI: 10.1021/jacs.6b08897
J. Am. Chem. Soc. 2016, 138, 14083−14091

species B. Furthermore, the steady state approximation for this pathway (eq 8) is distinct from the steady state approximation for a bidentate phosphine, and has the concentration of phosphine in the denominator. The phosphine concentration is very low, and the overall rate of decarbonylation with one phosphine associated should increase greatly compared to bidentate phosphines. This explains the inherent instability of Ni ketene complexes with monodentate phosphine ligands.

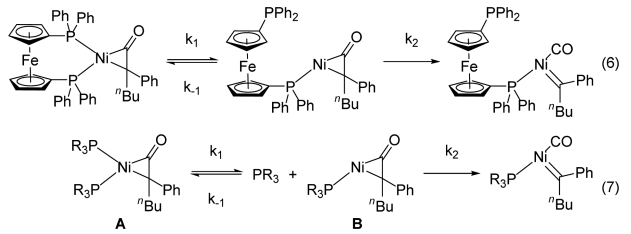

$$k = \frac{k_1 k_2[\mathbf{A}]}{k_{-1}[\mathbf{PR_3}] + k_2} \quad (8)$$

CONCLUSION

Dppf was discovered to be a uniquely suitable ligand for the generation of stable Ni−ketene complexes, and we were able to synthesize and characterize a library of (dppf)Ni[O=C=C(Ar)(R)] complexes. Crystallographic data reveals that the ketene is C=O coordinated with the ketene's aryl group distal to the Ni atom. Spectroscopic data reveal that the coordination mode observed in the solid state predominates in solution; however, C=O coordination with the aryl group oriented toward the (dppf)Ni fragment and C=C coordination are both observed. A combined experimental and theoretical approach was used to elucidate the mechanism of decomposition of these complexes which involves a rate-determining step of either decarbonylation or hydride transfer. That is, decarbonylation was determined to be the rate-determining step for **8b** through kinetic isotope effect and Mayer bond order analyses. Similarly, a LFER for **8cb**−**8cd** combined with Mulliken analysis suggested decarbonylation and not hydride migration was rate limiting for these complexes. Electron poor and sterically large ketenes decompose with rates that do not fit the trends for the complexes with rate limiting decarbonylation. Our computational model provided a rationale for why the hydride transfer is attenuated and becomes rate limiting in these cases.

Importantly, our calculations revealed that the Ni center is reduced during decarbonylation. We believe that more electron rich phosphines should further stabilize Ni−ketene complexes and are currently investigating this hypothesis. Furthermore, decarbonylation is more facile with one phosphine associated, explaining the instability of known Ni−ketene complexes with monodentate phosphines.

This report bridges the gap between the instability of the known Ni−ketene complexes and their use as intermediates in synthesis. We believe that knowledge of the mechanism of decomposition of Ni−ketene complexes, particularly the fact that bidentate phosphines stabilize these complexes, will lead to improvement of known reactions of Ni−ketene complexes and aid in the development of further reactions that use these complexes as intermediates.

ASSOCIATED CONTENT

Supporting Information

The Supporting Information is available free of charge on the ACS Publications website at DOI: 10.1021/jacs.6b08897.

Synthesis and characterization of (dppf)Ni(ketene) complexes (NMR, and X-ray data), NMR/IR scale experiments with other phosphines, kinetic analyses, computational data (PDF)
NMR data (PDF)
Crystal data for **8a** (CIF)
Crystal data **8b** (CIF)
Crystal data **8e** (CIF)
Crystal data **8ca** (CIF)
Crystal data **8cb** (CIF)
Crystal data **8cc** (CIF)

AUTHOR INFORMATION

Corresponding Author

*louie@chem.utah.edu

Notes

The authors declare no competing financial interest.

ACKNOWLEDGMENTS

We gratefully acknowledge the National Science Foundation (CHE1213774) and the National Institute of Health (GM076125) for financial support. N. D. Staudaher thanks Eastman Chemical Co. for a summer fellowship. We are grateful to Professor Matthew T. Kieber-Emmons for valuable discussions on computational chemistry. We also thank Joseph Lovelace for help synthesizing ketenes. Calculations were performed on the Extreme Science and Engineering Discovery Environment (XSEDE), which is supported by National Science Foundation (ACI-1053575).

REFERENCES

(1) Zhang, Z.; Zhang, Y.; Wang, J. *ACS Catal.* **2011**, *1*, 1621.
(2) Ruchardt, C.; Schrauzer, G. N. *Chem. Ber.* **1960**, *93*, 1840.
(3) (a) Auvinet, A. L.; Harrity, J. P. *Angew. Chem., Int. Ed.* **2011**, *50*, 2769. (b) Huffman, M. A.; Liebeskind, L. S. *J. Am. Chem. Soc.* **1991**, *113*, 2771.
(4) Kumar, P.; Troast, D. M.; Cella, R.; Louie, J. *J. Am. Chem. Soc.* **2011**, *133*, 7719.
(5) Rofer-DePoorter, C. K. *Chem. Rev.* **1981**, *81*, 447.
(6) Mindiola, D. J.; Hillhouse, G. L. *J. Am. Chem. Soc.* **2002**, *124*, 9976.
(7) Miyashita, A.; Sugai, R.; Yamamoto, J. *J. Organomet. Chem.* **1992**, *248*, 239.
(8) Hoberg, H.; Korff, J. *J. Organomet. Chem.* **1978**, *152*, 255.
(9) Hofmann, P.; Perez-Moya, L. A.; Stegelmann, O.; Riede, J. *Organometallics* **1992**, *11*, 1167.
(10) Curley, J. J.; Kitiachvili, K. D.; Waterman, R.; Hillhouse, G. L. *Organometallics* **2009**, *28*, 2568.
(11) Grotjahn, D. B.; Collins, L. S. B.; Wolpert, M.; Bikzhanova, G. A.; Lo, H. C.; Combs, D.; Hubbard, J. L. *J. Am. Chem. Soc.* **2001**, *123*, 8260.
(12) Grotjahn, D. B.; Bikzhanova, G. A.; Collins, L. S. B.; Concolino, T.; Lam, K.; Rheingold, A. L. *J. Am. Chem. Soc.* **2000**, *122*, 5222.
(13) Urtel, H.; Bikzhanova, G. A.; Grotjahn, D. B.; Hofmann, P. *Organometallics* **2001**, *20*, 3938.
(14) Ellgen, P. C. *Inorg. Chem.* **1971**, *10*, 232.
(15) Staudaher, N. D.; Stolley, R. M.; Louie, J. *Chem. Commun.* **2014**, *50*, 15577.
(16) Le Page, M. D.; Patrick, B. O.; Rettig, S. J.; James, B. R. *Inorg. Chim. Acta* **2015**, *431*, 276.

DOI: 10.1021/jacs.6b08897
J. Am. Chem. Soc. 2016, 138, 14083−14091

(17) Yin, G.; Kalvet, I.; Englert, U.; Schoenebeck, F. *J. Am. Chem. Soc.* **2015**, *137*, 4164.
(18) Sinnokrot, M. O.; Sherrill, C. D. *J. Phys. Chem. A* **2004**, *108*, 10200.
(19) (a) Bleuel, E.; Laubender, M.; Weberndorfer, B.; Werner, H. *Angew. Chem., Int. Ed.* **1999**, *38*, 156. (b) Cordaro, J. G.; van Halbeek, H.; Bergman, R. G. *Angew. Chem., Int. Ed.* **2004**, *43*, 6366. (c) Grotjahn, D. B.; Bikzhanova, G. A.; Hubbard, J. L. *Organometallics* **1999**, *18*, 8614.
(20) Wang, Y.; Agbossou, F.; Dalton, D. M.; Liu, Y.; Arif, A. M.; Gladysz, J. E. *Organometallics* **1993**, *12*, 2699.
(21) Barcs, B.; Kollár, L.; Kégl, T. *Organometallics* **2012**, *31*, 8082.

DOI: 10.1021/jacs.6b08897
J. Am. Chem. Soc. 2016, 138, 14083−14091